Carbon 173 (2021) 744–757

Contents lists available at ScienceDirect

Carbon

journal homepage: www.elsevier.com/locate/carbon

Research Article

Hard, transparent, sp^3-containing 2D phase formed from few-layer graphene under compression

Luiz G. Pimenta Martins [a, *], Diego L. Silva [b], Jesse S. Smith [c], Ang-Yu Lu [d], Cong Su [e], Marek Hempel [d], Connor Occhialini [a], Xiang Ji [d], Ricardo Pablo [e], Rafael S. Alencar [b], Alan C.R. Souza [b], Alysson A. Pinto [f], Alan B. de Oliveira [f], Ronaldo J.C. Batista [f], Tomás Palacios [d], Mário S.C. Mazzoni [b], Matheus J.S. Matos [f], Riccardo Comin [a], Jing Kong [d, **], Luiz G. Cançado [b, ***]

[a] Physics Department, Massachusetts Institute of Technology, Cambridge, MA, 02139, USA
[b] Departamento de Física, Universidade Federal de Minas Gerais, Belo Horizonte, MG, 30123-970, Brazil
[c] High Pressure Collaborative Access Team, X-ray Science Division, Argonne National Laboratory, Argonne, Illinois, 60439, USA
[d] Department of Electrical Engineering and Computer Science, Massachusetts Institute of Technology, Cambridge, MA, 02139, USA
[e] Department of Nuclear Science and Engineering, Massachusetts Institute of Technology, Cambridge, MA, 02139, USA
[f] Departamento de Física, Universidade Federal de Ouro Preto, Ouro Preto, MG, 35400-000, Brazil

ARTICLE INFO

Article history:
Received 16 September 2020
Received in revised form
5 November 2020
Accepted 12 November 2020
Available online 19 November 2020

ABSTRACT

Despite several theoretically proposed two-dimensional (2D) diamond structures, experimental efforts to obtain such structures are in initial stage. Recent high-pressure experiments provided significant advancements in the field, however, expected properties of a 2D-like diamond such as sp^3 content, transparency and hardness, have not been observed together in a compressed graphene system. Here, we compress few-layer graphene samples on SiO_2/Si substrate in water and provide experimental evidence for the formation of a quenchable hard, transparent, sp^3-containing 2D phase. Our Raman spectroscopy data indicates phase transition and a surprisingly similar critical pressure for two-, five-layer graphene and graphite in the 4–6 GPa range, as evidenced by changes in several Raman features, combined with a lack of evidence of significant pressure gradients or local non-hydrostatic stress components of the pressure medium up to ≈ 8 GPa. The new phase is transparent and hard, as evidenced from indentation marks on the SiO_2 substrate, a material considerably harder than graphene systems. Furthermore, we report the lowest critical pressure (≈ 4 GPa) in graphite, which we attribute to the role of water in facilitating the phase transition. Theoretical calculations and experimental data indicate a novel, surface-to-bulk phase transition mechanism that gives hint of diamondene formation.

1. Introduction

The search for stable 2D diamond has gathered recent interest due to the possibility of combining diamond's distinguished properties, such as superior hardness [1] and heat conduction [2], to exotic new properties that may arise from the reduced dimensionality. Its existence was first proposed over a decade ago [3] and different structures have been theoretically proposed ever since [4–7]. In most structures, stability is achieved by surface functionalization at the top and bottom surfaces [3,6,7], sometimes called diamane [3] for bilayer, and diamanoïds for thicker layers [8]. Diamondene [9], another proposed 2D diamond structure, greatly differs from those, being covalently bonded to chemical groups only at the top surface while the bottom exhibits a periodic array of dangling bonds. For a complete top surface-functionalization, this structure is predicted to be stable upon pressure release and the dangling bonds can be preserved if the substrate is chemically inert. These unpaired electrons generate magnetism in diamondene, and their periodic distribution gives rise to two spin-polarized bands, making it an ideal platform material for spintronics [5,9].

* Corresponding author.
** Corresponding author.
*** Corresponding author.
E-mail addresses: lmartins@mit.edu (L.G. Pimenta Martins), jingkong@mit.edu (J. Kong), cancado@fisica.ufmg.br (L.G. Cançado).

https://doi.org/10.1016/j.carbon.2020.11.038
0008-6223/

In this brand new and fast-moving field of 2D diamond research, there are two main routes being explored for synthesis: high-pressure compression and chemical functionalization of few-layer graphene. On the chemical functionalization front, the strongest indications of the existence of 2D diamond had been obtained from Raman spectroscopy measurements of hydrogenated few-layer graphene [8,10]. Recently, Bakharev et al. [11] provided convincing structural evidence for the formation of diamane through fluorination of bi-layer graphene. However, their samples did not show any Raman feature of diamond, unlike the diamond features observed for hydrogenated graphene in the work by Piazza et al. [8]. Considering both works used similar excitation laser energies (in the visible range), such discrepancy indicates that there are open questions regarding the properties of different 2D diamond structures.

On the high-pressure front, most experimental indications of the existence of 2D diamond have been obtained either by tip-compression [5,7,12] or hydrostatic compression [9,13,14] of few-layer graphene. Even though the aforementioned works reporting on the tip-compression route provide significant advances in the field, the resulting pressure-induced phase is spatially limited to the size of the apex of the compressing tip, which limits potential applications and makes it challenging to further assess the resulting structural properties. As a most reliable alternative, hydrostatic compression using diamond anvil cells (DACs) allows for the pressure-induced conversion of the whole flake, facilitating the investigation of the material properties of the pressure-induced phase and opening the possibility of obtaining stable structures for practical applications. To date, there are only a few reports on pressure-induced transformations in individual graphene films using DACs [9,13,14], in contrast with the vast literature describing high-pressure phases in room-temperature compressed graphite [15–20].

Martins et al. [9], performed high-pressure Raman experiments on CVD graphene samples, monitoring the bond-stretching G mode's frequency with laser energy. The G peak blueshifts for higher excitation energy in a mixed sp^2-sp^3 system, whereas its position is independent of the laser excitation energy in a pure sp^2 system [21]. From those measurements, the authors observed a sp^2 to sp^2-sp^3 phase transition at $\approx$ 5 and 7.5 GPa in double-layer CVD graphene for two samples when water was used as the pressure transmitting medium (PTM). The transition was not observed for single layer graphene compressed in water PTM or bi-layer graphene compressed in mineral oil up to $\approx$ 13 GPa. Those results indicate that water facilitates the phase transition in graphene systems with two or more layers, by reducing the critical pressure. Indeed, tip-compression measurements also indicated a water-assisted pressure-induced phase transition in graphene with two or more layers [5] as well as in hexagonal boron nitride (hBN) [22], being absent in dry conditions for both cases.

The proposed mechanism for this water-assisted pressure-induced phase transition in graphene is that under high pressures, water can provide the functionalization groups −H or −OH that can bond to the top graphene layer, substantially decreasing the pressure necessary to form inter-layer covalent bonds between the carbon atoms [5,9], leading to the formation of diamondene. Such a mechanism could explain the large discrepancy in critical pressures observed for bi-layer graphene compressed in water ($\approx$ 6 GPa) [9] compared to tri-, tetra-, hexa-, and 12-layer graphene compressed in Daphne 7373/Argon PTMs ($\approx$ 20–30 GPa) [13,14].

In Ref. [13], the authors observed band gap opening accompanied by transparency starting at $\approx$ 30 GPa in tri-layer graphene from electrical resistance and optical absorption measurements [13], which they inferred that could be caused by a sp^2-sp^3 rehybridization. More recently, the same group repeated the methodology to detect band gap opening in tri-, tetra-, hexa- and 12-layer graphene in the $\approx$ 20–30 GPa range [14]. They associated this transformation to the formation of an atomically thin hexagonal diamond. However, it is important to note that the claim was based on experimental data obtained from x-ray diffraction (XRD) measurements performed on graphene powder, which is a mixed system with flakes of different thicknesses randomly stacked on top of each other. Therefore, one cannot rule out the possibility that the observed hexagonal diamond diffraction signal originates from bulk structures formed upon coalescence of several flakes, or from transformation of thicker graphite flakes usually present in graphene powders. In fact, it must be pointed out that in-situ structural evidence of an isolated 2D diamond formed by compression of isolated flakes via high-pressure experiments presents an enormous challenge given the 2D nature of the samples and their low atomic number.

From the combined information from these aforementioned works, pressure-induced transparency and evidence of a sp^3-rich phase have each been reported individually in Refs. [13,14] and Ref. [9], respectively. It is important to mention that even though transparency could be an indication of sp^2-sp^3 phase transition, the experimental techniques used in Refs. [13,14] do not allow to assess the presence of sp^2 and sp^3 carbons, unlike Raman spectroscopy. Evidence of increased hardness has been reported only by local nano-indentation experiments in bilayer graphene on SiC [7], and was not accompanied by further information about optical properties or spectroscopic signatures of the new phase. It is still possible that the observed features in these works are uncorrelated to a phase transition to a 2D diamond-like phase. Thus, the combined properties expected from a 2D diamond-like structure, such as sp^3 content, transparency and hardness, have not yet been observed in compressed graphene systems.

In this work, few-layer graphene samples on SiO_2/Si substrate are compressed in a water PTM. The first experimental evidence of the formation of a quenchable pressure-induced hard, transparent, sp^3-rich 2D phase is provided from changes in the Raman spectra and optical images upon compression as well as from indentation marks on the substrate, as evidenced by atomic force microscopy (AFM) measurments of the samples post-compression. For optical measurements, we developed a new technique to consistently load 2D materials on SiO_2/Si substrate into diamond anvil cells (DACs). The Raman spectroscopy results indicate a surprisingly similar critical pressure for two- and five-layer graphene, and also for thin graphite (more than 20 layers) in the 4–6 GPa range, as well as the lowest reported critical pressure ($\approx$ 4 GPa) and pressure-induced transparency (completed at $\approx$ 7 GPa) in graphite, which we attribute to the role of water in facilitating the phase transition. Molecular Dynamics (MD) and Density Functional Theory (DFT) simulations show a surface-to-bulk phase transition mechanism that starts with the inter-layer bonding of the top layers and then propagates along the *c* axis with increasing pressure. Our experimental data corroborates with this mechanism, giving hints of diamondene formation at the onset of the phase transition.

2. Experimental details

2.1. Sample preparation - mechanically exfoliated graphene

High-pressure Raman experiments were performed on mechanically exfoliated graphene samples sitting on SiO_2/Si substrates. To prepare the samples, we developed a new method that can be used to systematically load 2D materials and related heterostructures into DACs, addressing a common bottleneck in high-pressure experiments involving these types of systems. Horseshoe-shaped trenches were etched through 25 μm-thick Si

substrates covered with a 300 nm-thick SiO_2 layer, as shown in Fig. 1 (a). The graphene flakes were transferred onto the region surrounded by the trenches, using a pick–up/transfer technique [23]. Afterwards, the tiny ($\approx$ 70 μm of diameter) SiO_2/Si disk supporting the graphene piece was cleaved and detached from the SiO_2/Si wafer using a sharp stainless steel tip, and the same tip was used to bring the disk inside the DAC, as illustrated in Fig. 1(b). For the Raman experiments, two samples were prepared using this method: a bi-layer graphene, shown in Fig. 1(c), and a thin graphite (much more than 20 layers) piece sitting next to a five-layer graphene, both shown in Fig. 1(d).

The samples were compressed in the DAC using water as the PTM, and all Raman spectra were acquired using a 532 nm excitation laser wavelength [schematics shown in Fig. 1(e)]. Fig. 1(f) shows the evolution with pressure of the first-order Raman-allowed G band ($\approx$ 1580 cm^{-1} in ambient pressure), and the two-phonon Raman 2D band ($\approx$ 2700 cm^{-1}) [24] for the five-layer graphene sample compressed in water PTM up to 18 GPa. The strong Raman features at approximately 1330 cm^{-1} and below 2670 cm^{-1} correspond to a first and a second-order Raman mode of diamond, respectively, originated from the top diamond of the DAC. The hydrostatic limit of water is an important issue to be addressed in our experiment, and it will be discussed in detail along the text and in the Supplemental Information.

2.2. Sample preparation - graphene powder

The graphene powder was prepared by liquid–phase exfoliation of natural graphite. The sample was centrifuged at 15,000 *g*. Statistical AFM analysis [49] was carried out over more than 4,000 flakes, and the results show that $\approx$ 25% of the sample, in mass, is composed of few-layer graphene flakes (less than 5 layers), $\approx$ 35% is composed of graphene platelets with thicknesses between 6 and 10 layers, $\approx$ 26% is composed of platelets with thicknesses between 10 and 20 layers, and $\approx$ 14% of flakes with more than 20 layers. In fact, from the XRD data taken at ambient pressure, one can notice that the G002 and G101 peaks from graphene are broad, an indication of a poor degree of crystallinity along *c* axis, as expected for a powder composed of randomly stacked 2D flakes. To avoid the presence of residual water content and reagents, the sample was calcinated at 400 °C.

2.3. High-pressure Raman

Raman spectra were acquired using an alpha 300 system RA from WITec (Ulm, Germany) equipped with a highly linear (0.02%) piezo-driven stage, and objective lenses from Nikon (10 $\times$, NA = 0.3 for high-pressure measurements and 50 $\times$, NA = 0.55 for room condition measurements). A diode pumped solid state polarized laser, λ = 532 nm, was used. The incident laser was focused with a diffraction-limited spot size (0.61λ/NA), and the Raman signal was detected by a high-sensitivity, back-illuminated CCD located behind a 600 g/mm grating. The spectrometer used was an ultra-high throughput Witec UHTS 300 with up to 70% throughput, designed specifically for Raman microscopy. To avoid damage due to sample heating, measurements were performed with powers of approximately 3 mW and 9 mW for the 50 $\times$ and 10 $\times$ objective lenses, respectively.

High-pressure Raman measurements were performed with a gas-membrane driven DAC, microScope DAC-HT(G), using Inconel 718 pre-indented ($\sim$ 90 μm) gaskets. It is important to note that at pressures below 3 GPa, the 2D peak partially overlaps with the second-order Raman peak originated from the DAC's diamond anvils. The pressure was monitored using the ruby's calibration method described in Ref. [50]. The spectra of G and 2D bands were fitted with Voigt functions using the software PeakFit v4.12. The

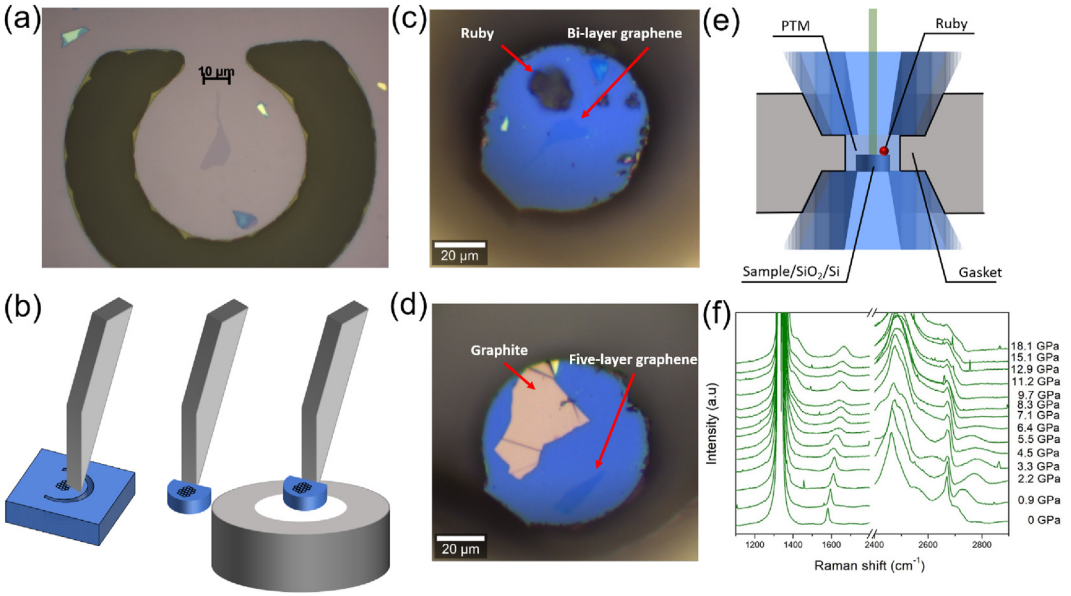

Fig. 1. Horseshoe method to load 2D materials transferred onto SiO_2/Si substrates into DACs. (a) Optical image of a bi-layer graphene sample on a silicon disk. A "horseshoe" shape is etched through a 25 μm silicon sample coated with a 300 nm thermal oxide. Then, the 2D sample is transferred onto the center of the silicon disk via the standard pick up and transfer technique. (b) Illustration of the "breaking and loading" process. First, the silicon disk containing the sample is pressed with the tip of a needle, in a region away from the sample, until it cleaves. The sample/SiO_2/Si is then picked up, and loaded into the gasket hole with the aid of a needle. (c–d) Optical images of the samples inside the gasket hole of bi-layer graphene (c) and five-layer graphene and graphite (d). (e) Schematic of the high-pressure Raman experiments. The sample was loaded into a DAC together with the ruby and water PTM. At each pressure, the Raman spectra were acquired with a 532 nm laser excitation line. (f) Evolution of the G and 2D bands (at $\approx$. 1580 and $\approx$. 2700 cm^{-1} at ambient pressure, respectively) with pressure for the five-layer graphene sample compressed in water PTM up to 18 GPa. The strong Raman features at approximately 1330 cm^{-1} and in the range of 2400–2670 cm^{-1} correspond to the first and second-order Raman modes originated from the top diamond of the DAC. (A colour version of this figure can be viewed online.)

numbers of layers of graphene samples were determined by standardized principal component analysis (PCA) of the 2D band [51].

2.4. Experiments to confirm the indentation

The high-pressure compression of the four-layer graphene and graphite on SiO_2 substrate was performed with a Symmetric type DAC, using stainless steel pre-indented ($\sim$ 90μm) gaskets. The pressure was increased to 8 GPa and kept at this pressure for 12 h, after which the DAC was opened, the sample was recovered, and its Raman spectra collected. No Raman spectrum was acquired during compression. Raman spectra were acquired after decompression using a confocal microscope spectrometer (Horiba LabRAM HR Evolution) in a backscattering geometry, with a 50 $\times$ objective lens and 532 nm excitation laser source. The measurement was performed with a laser power of approximately 3 mW to avoid damage due to sample heating. The AFM topography measurement of the recovered samples was performed with a Cypher S AFM Microsope using an AC240TS-R3 cantilever from Oxford Instruments, with resonance frequency at 70 Hz.

2.5. High-pressure x-ray diffraction

High-pressure XRD measurements were conducted at 16ID-B of High Pressure Collaborative Access Team (HPCAT) at the Advanced Photon Source (APS), Argonne National Laboratory, using a symmetric type DAC. The incident monochromatic x-ray beam, $\lambda =$ 0.40663 Å was focused down to 5–10 μm in diameter, and the XRD patterns were collected by a Pilatus Area Detector. The XRD spectra were analyzed using Matlab for background subtraction and PeakFit v4.12 for Voight fit of the G002 peak.

3. Theoretical calculations details

In the MD simulations, performed with the LAMMPS [52] software, atoms were treated as point particles interacting through the AIREBO [53] potential. The H-functionalized five-layer graphene was represented by 22,880 and 2,288 carbon and hydrogen atoms, respectively, and boundary conditions were imposed in the in-plane x- and y-directions. The time step was set to 0.25 fs. We employed the Nosé-Hoover thermostat [54] scheme to keep the average temperature at 300 K. Additionally, the Nosé-Hoover barostat was used in order to allow for fluctuations in the lateral (xy) box dimensions (external pressure set to 1 bar). The five layers were placed in the AB-stacking, with a repulsive wall placed immediately bellow the fifth layer. The pressure was applied to the system by a moving piston modeled as a Lennard-Jones (LJ) wall, initially placed 4 Å above hydrogen atoms, with energy and distance parameters of 1.0 meV and 3.0 Å, respectively. Simulations were divided in two stages, the preparation and production ones. The preparation stage comprised a structure minimization followed by a temperature equilibration dynamic, in which the system was linearly heated from 30 K to 300 K during 25 ps and kept at this temperature for further 25 ps. In the first part of the production stage (loading process), the distance between the piston and the system was linearly decreased during 200 ps, leaving an average graphene interlayer separation of 2.6 Å. Piston position was kept for 400 ps, and then returned to its initial position after additional 100 ps.

In the spin-DFT [55,56] calculations, we employed the SIESTA implementation [57], making use of norm conserving Troullier-Martins pseudopotentials [58] in the factorized Kleinman-Bylander form [59]. The basis set was composed of double-zeta pseudoatomic orbitals of finite range augmented by polarization functions - the DZP basis set. The generalized gradient approximation (GGA) [60] was chosen to represent the exchange-correlation functional. We performed integrals in real space using a grid defined by a meshcutoff of 350 Ry, and the Brillouin zone was sampled using a k-grid cutoff of 30 Å. The geometries were considered optimized when the maximum force component (not constrained) in any atom was less than 10 meV/Å. To mimic the application of pressure, we employ a hard-wall constraint in the lowest carbon atoms, which are not allowed to move in the negative z-direction, while a predefined force is applied in the oxygen atoms of the −OH groups which functionalize the upper graphene surface.

For the Young Modulus calculations, we applied strains up to 2% in the zig-zag and armchair direcitons, and up to 2% in the calculations of the transverse Young modulus. The bulk modulus calculations were performed by varying the lattice vectors up to strains of 4% (in steps of 0.5%). The stacking orders were AB, ABB, ABBB and ABCCB from bi-layer to five-layer diamondene, respectively.

In the MD simulations, we chose hydrogen functionalization of the upper graphene layer, since model potentials for C−H bonds are well described in literature. First principles calculations can be performed with either −OH and −H groups, rendering basically the same results. We chose −OH to be consistent with similar models reported in previous studies [5,9].

For plotting the LDOS of the dangling bonds in Fig. 3(b and c), the Xcrysden program was used [61]. An isovalue of 0.01 was used in Figs. 3(b) and 0.015 in Fig. 3(c).

4. Results and discussion

Fig. 2(a–c) show selected Raman spectra of the compressed bi-layer graphene, five-layer graphene and thin graphite, respectively, measured at different pressures featuring the G and 2D bands. Fig. 2(d–f) show the plot of the pressure-evolution of the G and 2D band frequencies subtracted from their frequencies measured in ambient conditions ($\Delta\omega_G$ and $\Delta\omega_{2D}$, respectively). The data were extracted from the Raman spectra of bilayer graphene, five-layer graphene and graphite, respectively. Fig. 2(d–f) further show the evolution of the full-width at half maximum of the G band, $\Delta\Gamma_G$. Fig. 2(g–i) show the ratio between 2D and G bands intensities, I_{2D}/I_G, as a function of pressure, for the bilayer graphene, five-layer graphene and graphite, respectively.

In the pressure range from 0 to $\approx$ 6 GPa for bi-layer graphene, from 0 to $\approx$ 4 GPa for five-layer graphene, and from 0 to $\approx$ 3 GPa for thin graphite, we observe the expected strain-induced phonon hardening [25], manifested through linear blueshifts of G and 2D bands [26]. Also, in the same range of 0−$\approx$ 6 GPa for bi-layer graphene we observed that the linear shifts of G and 2D bands occur without significant changes in their relative intensities or in Γ_G [27], whereas we observed a gradual decrease of 2D band intensity and gradual increase of G band width for five-layer graphene and thin graphite.

However, this trend suddenly changes at $\approx$ 6 GPa for bi-layer graphene and at $\approx$ 4 GPa for five-layer graphene and thin graphite. As can be seen in Fig. 2(a,d), between 6.05 and 6.35 GPa the bi-layer graphene spectra shows a simultaneous abrupt G band broadening and a redshift of 6.2 cm^{-1} along with a sudden drop in the 2D band's intensity and drastic 2D band's redshift. Such changes are highlighted in Fig. 2(d,g) by the black-dashed line. Unlike the bi-layer graphene case, the experimental data obtained from five-layer graphene and graphite do not demonstrate a clear trend for a redshift in ω_G, although there are indications that similar changes may have occurred. Between 3.3 GPa and 4.5 GPa, the G band's frequency of five-layer graphene changed from 1613.0 cm^{-1}–1608.1 cm^{-1}, a redshift of 4.9 cm^{-1} in a range of

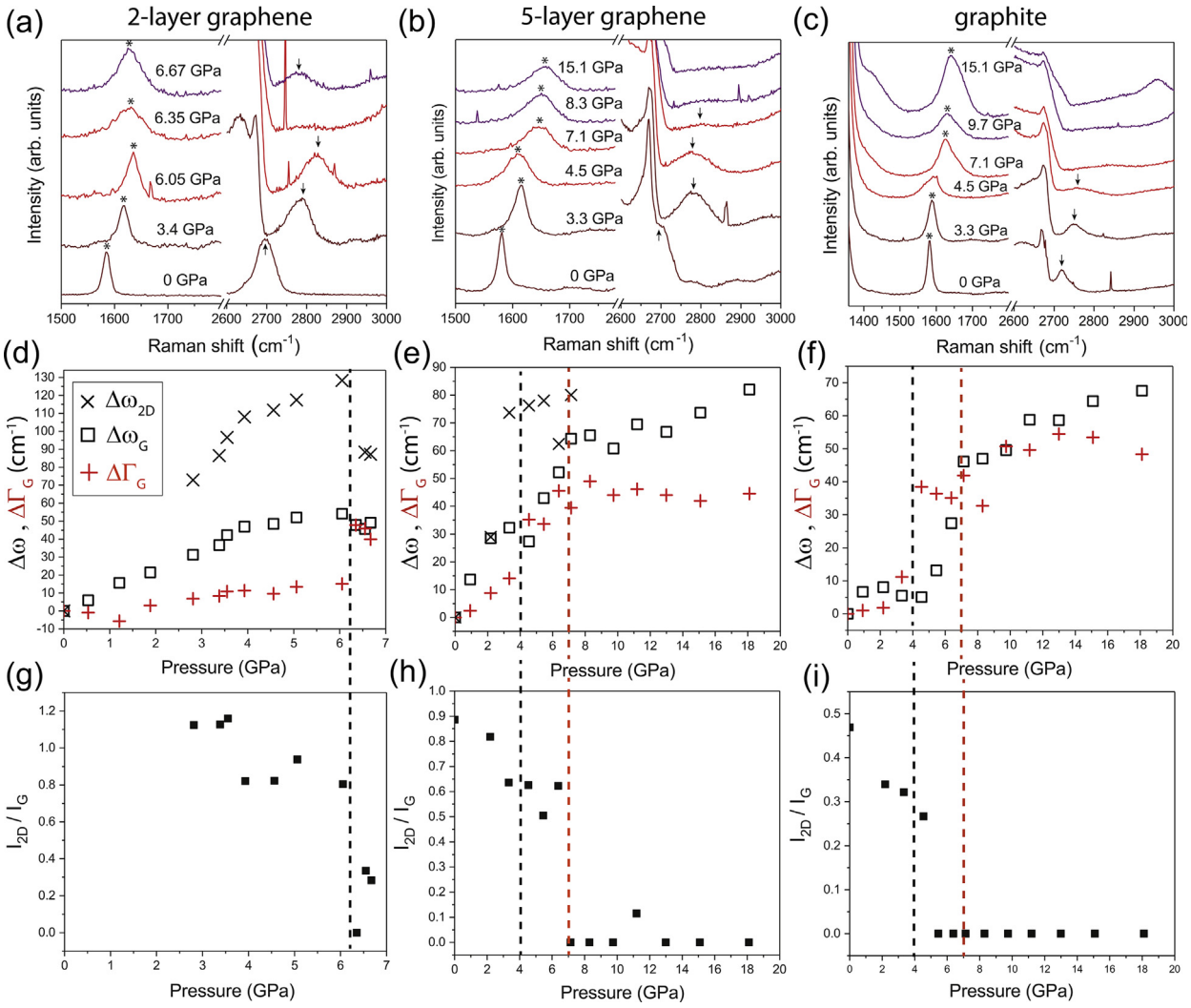

Fig. 2. Phase transition evidence obtained from Raman spectroscopy. (a–c) Selected Raman spectra at different pressures for (a) bilayer graphene, (b) five-layer graphene and (c) graphite. G and 2D bands are indicated with * and ↓, respectively. (d–f) Plots of the G (2D) band frequency and full width at half maximum subtracted from their values at initial pressure, $\Delta\omega_G$ ($\Delta\omega_{2D}$), and $\Delta\Gamma_G$, respectively, as a function of pressure for (d) bilayer graphene, (e) five-layer graphene and (f) graphite. The black-dashed lines indicate the critical pressures of the phase transition, whereas the red-dashed lines indicate the end of the phase transition. (g–i) Plots of the intensity ratio between the 2D and G band (I_{2D}/I_G) for (g) bilayer graphene, (h) five-layer graphene and (i) graphite. Data from 2D band for bi-layer graphene between 0 and approximately 3 GPa was not included since 2D peak partially overlaps with the second-order Raman peak originated from the DAC's diamond window in this pressure range. (A colour version of this figure can be viewed online.)

1.2 GPa. The redshift for the graphite flake is less pronounced and occurred between 2.19 GPa and 3.33 GPa, with G band's frequency changing from 1588.3 cm^{-1}–1585.7 cm^{-1}. Furthermore, both samples showed an abrupt broadening of G band at ≈ 4 GPa, as indicated by the black-dashed lines in Fig. 2(e and f), accompanied by an increase in the ω_G *vs P* slope in the 4–7 GPa range. For the graphite case, those changes were also accompanied by an abrupt 2D band's suppression at ≈ 4 GPa, while for five-layer graphene, the 2D band's intensity suppression occurred at ≈ 7 GPa, as can be seen in Fig. 2(h and i). Above 7 GPa, we observe a decrease in the ω_G *vs P* slope and we no longer observe a considerable broadening of G band for both five-layer graphene and graphite. Those changes are indicated by red-dashed lines in Fig. 2(e–i).

We now focus on understanding the origin of the observed changes in the Raman spectra depicted in Fig. 2. A possible cause for G band broadening could be the presence of pressure gradients or local non-hydrostatic stress components from the PTM, that could generate structural distortions in the graphene lattice. However, even though water becomes Ice VI at ≈ 1 GPa and Ice VII at ≈ 2 GPa [28] at room temperature, related literature [28–30] as well as our own data show a lack of evidence of significant pressure gradients or local non-hydrostatic stress components in water up to approximately 8 GPa. Here we discuss the main points which are relevant to our analysis. The detailed discussion on the hydrostatic limits of water is presented in Section 1 in the Supplemental Material. Piermarini et al. [29] investigated the hydrostatic limit of water, among other PTMs, in DAC experiments using two methods: by measuring the pressure at several different locations from ruby crystals spread across the chamber, and by measuring the spectral linewidth of the R_1 fluorescence peak from ruby. From the first method, they observed practically no pressure gradient up to approximately 8 GPa in compressed water and a presence of a low-pressure gradient of $\delta P \approx$ 1 GPa from 8 to 14 GPa. From the second method, they observed an increase in linewidth associated with local non-hydrostatic stress components that is consistent with the observations from their first method, with local non-hydrostatic stress components of only 0.6 GPa at 9.2 GPa.

Our analyses of the linewidth of the R_1 and of the difference in peak position between R_1 and R_2 ruby fluorescence peaks support those observations (see Fig. S1 in the Supplemental Material). The

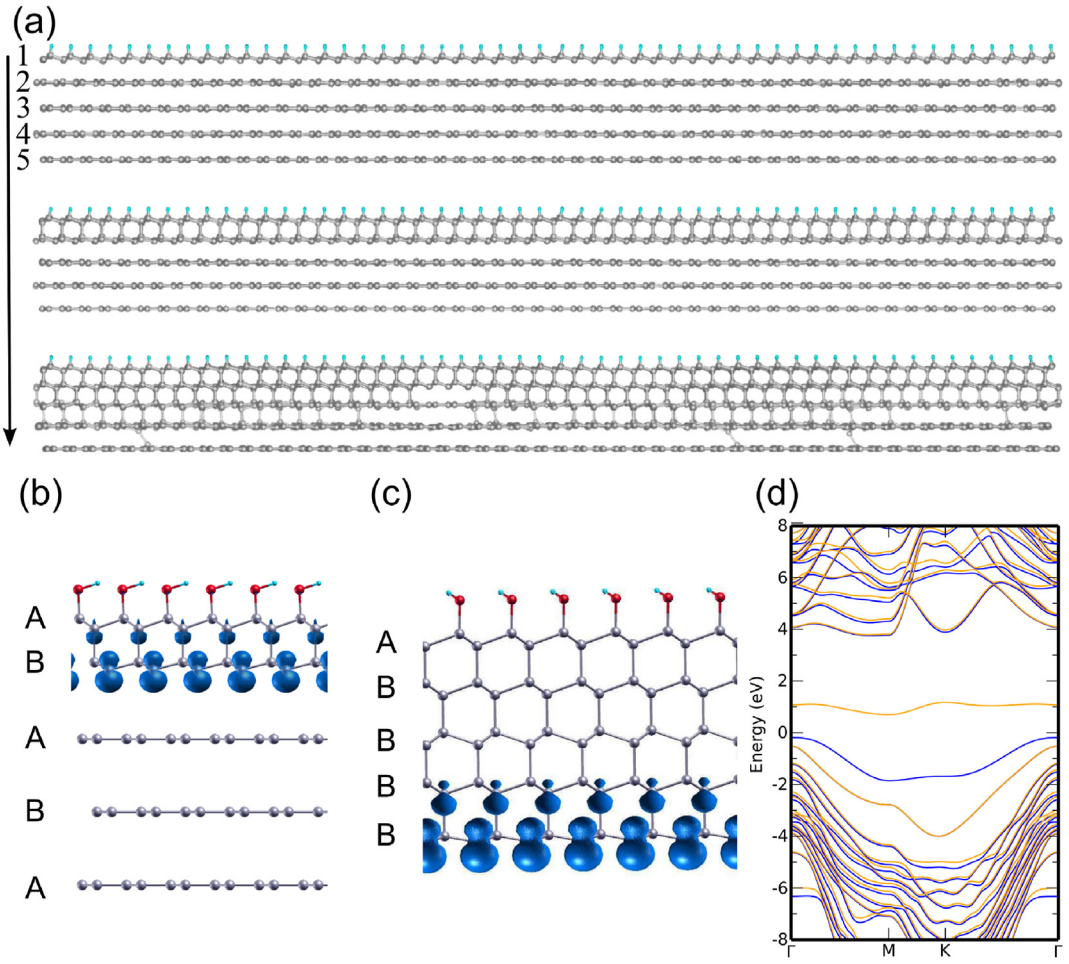

Fig. 3. Evolution of the sp^2–sp^3 restructuring process. (a) Snapshots of the MD simulation of a five-layer graphene system with increasing pressure. After formation of diamondene, the process propagates to other layers through formation of interlayer covalent bonds. (b,c) DFT results with increasing applied force, also showing the Local Density of States (LDOS) of the dangling bonds above Fermi level. Interestingly, a similar structure has been recently reported from hot-filament process of few-layer graphene [10]. In the last configuration, the system is completely rehybridized, and the staking order is ABBBB. In the BB part of that stacking, the interlayer bonds are in an eclipsed conformation. (d) Band structure for the complete sp^3 configuration. Blue and yellow lines represent the two spin components. The system is a ferromagnetic semiconductor with a band gap of 0.88 eV. A magnetic moment of 1 μ_B is associated with each primitive cell. (A colour version of this figure can be viewed online.)

lack of pressure gradients in the 0–8 GPa range was confirmed by an additional high-pressure Raman experiment using water as the PTM (see details in Section 1 of the Supplemental Material). Given that the observed changes in the Raman spectra of the flakes occurred below 7 GPa, such drastic changes can not be explained by possible pressure gradients or local non-hydrostatic stress components from the PTM. Moreover, if such changes were caused by structural disorder induced by the PTM, they should be more pronounced as the non-hydrostatic stress components starts to appear, which happens above ≈ 8 GPa. In fact, our data reveals an opposite behavior: G band width becomes approximately constant and we no longer observed deviations from the linear behavior in $d\omega_G/dP$ above 7 GPa.

G band broadening and 2D band suppression could also arise due to a differential compressibility between Ice VII and SiO_2 substrates, which would generate in-plane shear components that could rip and cause structural distortions in the graphene lattice. However, this situation is unlikely due to the remarkable resemblance between the differential compressibility between Ice VII and SiO_2 substrates in the 0–8 GPa range [31].

The sudden redshift of G band observed for the bi-layer flake could in principle be associated with sample detachment from the substrate. Filintoglou et al. [27] observed an abrupt decrease of the G band's frequency accompanied by a reduction of the pressure slope ($d\omega_G/dP$) in monolayer graphene compressed above 2 GPa, which was attributed to graphene's detachment from the substrate. However, the main difference between our results and this previous work is that, in our case, the observed redshift in ω_G for bilayer graphene was accompanied by an abrupt G band broadening and 2D band suppression, which was not observed in the work of Filintoglou et al. [27]. In Ref. [27] the G bandwidth and the relative intensity of G and 2D bands do not change significantly during the whole compression run.

Furthermore, the authors relate such redshift of ω_G and change of ($d\omega_G/dP$) to graphene not being preferably adhered neither to the substrate nor the PTM, with its mechanical response to compression resembling that of a free-standing sample, thereby explaining the reduced slope. Such mechanism should indeed not change the G bandwidth or reduce 2D band intensity, since it only changes the in-plane strain transfer from substrate to graphene, therefore affecting the phonon frequencies and not necessarily the lifetime. One could also associate the change of G band frequency vs. pressure slope observed for five-layer graphene and graphite to sample detachment. However, unlike the work of Filintoglou et al. [27], we observed an increase in $d\omega_G/dP$, not a decrease, and it was accompanied by a drastic G band broadening, which was not observed in their work.

All together, we observed several changes in the Raman spectra of the flakes in the 0–7 GPa range. For bi-layer graphene, we observed a simultaneous abrupt broadening and redshift of G band, and 2D band suppression around 6 GPa. For five-layer graphene, we observed an abrupt broadening around 4 GPa, followed by an increase in G band frequency *vs* pressure slope above this pressure, and eventual 2D band suppression at ≈ 7 GPa. For graphite, we observed a G band broadening at 4 GPa, followed by an increase in G band frequency *vs* pressure slope and 2D band suppression above 4 GPa. Those changes in the Raman spectra of the flakes, combined with the lack of indications of pressure gradients or local non-hydrostatic stress components from PTM or shear components induced by differential compressibility between Ice VII and SiO_2, provide strong indication of a sp^2 to sp^2-sp^3 phase transition.

An increase in Γ_G is considered a signature of structural phase transitions in compressed graphite [16,32,33], and it is associated with the formation of sp^3 sites at the onset of phase transition [16]. For bilayer graphene, G band broadening occurs at approx. 6 GPa. For both five-layer [Fig. 2(b,e)] and graphite [Fig. 2c,f], Γ_G suddenly broadens around 4 GPa, indicating the onset of a phase transition, and remains relatively constant above 7 GPa, indicating a complete transition. Intensity suppression of 2D band is another evidence of phase transition. Because this Raman feature originates from double-resonance mechanisms [24], its intensity is highly sensitive to variations in the electronic and vibrational spectra caused by structural changes [34].

The slope of G band's frequency with pressure is associated with the compressibility of graphene [26], which is mediated by the strain transfer from the substrate [27,31]. As previously discussed, sample detachment is unlikely and based on previous investigations, there are no indications of charge transferring from the PTM affecting the pressure evolution of ω_G [27]. Therefore, the observed changes in slope of G band frequency with pressure in our data also provides additional evidence of phase transition. The steep ω_G *vs* P slope observed for the thin graphite flake - when compared to literature data - will be discussed later in the context of the surface-to-bulk phase transition mechanism.

We emphasize that the evidence of phase transition from Raman spectroscopy obtained for all samples occurred below 8 GPa. As previously discussed here and in Sec.1 of the Supplemental Information, literature data (Refs. [28–30]) as well as our data on R1 linewidth of Ruby fluorescence peak and G band frequency measured at different positions in a graphene powder show no evidence of significant pressure gradients or local-non hydrostatic stress components in water PTM in that pressure range that could explain such drastic changes. Furthermore, if such changes were caused by non-hydrostatic components from the water PTM, drastic changes for monolayer graphene compressed in water should have also been observed in the same pressure range. However in Martins et al. [9], the authors observed no significant changes in the Raman spectra of monolayer graphene compressed in water PTM up to 13 GPa: no G band dispersion with laser excitation energy, nor changes in the linear behavior of $d\omega_G/\ dP$. The observed G band broadening for that sample was likely caused by strain and stress gradients from the flexible Teflon substrate.

Furthermore, in Martins et al. [9] the authors have detected phase transition in bi-layer graphene (compressed in water PTM) in the same pressure range as in the current work, by measuring G band dispersion with different laser lines. The fact that the laser spot for the different laser excitation energies was placed at the same spot in the sample, ruled out the possibility that the changes were caused by non-hydrostatic behavior from the PTM since, if that was the cause, the G bands frequency should be the same regardless the laser energy. The fact that we observed increased transparency correlated to changes in the Raman spectrum, as it will be later shown, further reinforces the evidence of phase transition. Lastly, as it will be shown later, the fact that we observed that four-layer graphene and graphite flakes sink into the SiO_2 after compression, as revealed form AFM images (the samples were compressed up to 8 GPa), could not possibly be explained by the presence of non-hydrostatic stress components from the PTM. Therefore, the Raman changes are associated with a phase transition and not from non-hydrostatic components from the PTM.

Above 8 GPa and between 15 GPa, where most of our data for 5-layer graphene and graphite was obtained, a 1–2.5 GPa pressure gradient from water PTM was reported by Piermarini et al. [29], which is consistent with our estimated pressure gradient of approx. 1.5 GPa obtained from measurements of G band frequency at different positions in the graphene powder (see Table S1 in the Supplemental Information). Local non-hydrostatic stress components in the 8–15 GPa range are in the order of approx. 1 GPa, according to our analysis of the variation of the R1 peak width shown for Experiment II in Fig. S1 in the Supplemental Information, which agree with the value estimated by Wolanin et al. [30] of 1 GPa at 10 GPa, and 2 GPa at 20 GPa. In this latter work, apart from the quantification, the authors identified the local stress component to be uniaxial along the loading direction of the DAC, as explained in Sec.1 of the Supplemental Information. The presence of these components could have affected the Raman spectra in this pressure range by causing further broadening of G band or changes in the linear behavior of $d\omega_G/dP$. However, we observe quite an opposite behavior: the G bandwidth remain relatively constant in the 8–15 GPa range for both 5-layer graphene and graphite, and we did not observe a change in the linear behavior of $d\omega_G/dP$. Therefore, it is likely that the value of such non-hydrostatic stress components and their uniaxial direction are too small to cause significant changes in the Raman spectra in pressure range covered in our experiments.

It should be noticed that the persistence of the G band - a signature of sp^2 hybridization - through all compression range provides clear evidence that the sp^3 conversion is not complete. However, previous investigations on pressure-induced phase transitions in room-temperature compressed graphite, indicate that the new phase is expected to present if not a full sp^3 conversion [32,35–37], at least a comparable number of sp^2 and sp^3 sites [38]. The physical picture is that, upon compression, the formation of one single sp^3 bond triggers the reconstruction across the flake through a cooperative phenomenon [39]. Therefore, a primarily sp^2 phase with some sp^3 sites is unlikely, and it is not consistent with our results of transparency and hardness that will be shown later. Our proposal goes the other way around: after phase transition, there are still sp^2 sites remaining inside a rehybridized sp^3 matrix, as indicated in Ref. [9]. According to DFT calculations [5], a complete sp^3 conversion would require all carbon atoms from one sublattice of the top layer to be covalently bonded to chemical groups such as –H or –OH. However, it is unlikely that this requirement was met under our experimental conditions due to the formation of ice above ≈ 1 GPa, which drastically reduces the mobility of water molecules on the graphene's surface. Moreover, remaining residues from the polymer used in the transfer process may also have prevented complete functionalization of the sample's surface.

In fact, the extraction of in-situ direct evidence of crystalline sp^3 carbon from high-pressure Raman spectroscopy measurements is extremely challenging due to several reasons. First, considering excitation in the visible range, the Raman cross-section for sp^3 carbon is greatly reduced when compared to sp^2 [8]. For instance, the cross-section for bulk diamond at 514 nm is approximately 50 times lower than that of graphite [40]. One should expect an even lower cross-section for an atomic thick diamond-like sample. Second, the first order Raman peak from the diamond window of the

DAC would overlap with an eventual first-order 2D diamond peak. Nevertheless, the totality of information extracted from the Raman spectroscopy data presented in Fig. 2 provides clear indications that a sharp structural phase transition occurs at 6.3 GPa for bilayer graphene, whereas for both five-layer graphene and thin graphite, a transition occurs over the range from ≈ 4 GPa to ≈ 7 GPa. To the best of our knowledge, 4 GPa is the lowest onset of phase transition reported for room-temperature compressed graphite; the onset usually ranges from 9 to 18 GPa [15–20] (see Table S2 in Supplemental Information). Moreover, as previously mentioned, the pressure-induced phase transition observed for three-, four-, six- and twelve-layer graphene compressed in either Daphne 7373 or Argon PTM was approximately in the 20–30 GPa range [13], which is considerably higher than the 4–7 GPa range obtained from compression in water PTM, as reported here and in Ref. [9]. Therefore, by comparing the onset of the phase transition in graphene systems compressed with water versus other PTMs, we note that compression in water leads to a reduced critical pressure for both few-layer graphene and graphite systems. Combined with previous studies [5,9,22] the observation of such a reduced critical pressure provides strong indication for the role of water in facilitating this phase transition.

Upon pressure release, the G band width returns to its approximate initial value and the 2D band intensity is recovered for all samples (Fig. S3), showing that the pressure-induced phase is quenched. However, irreversible changes also occurred such as the presence of strong and sharp defect-induced D and D′ Raman bands [24] for most of the recovered samples (Fig. S3), their Raman spectra resembling that of partially functionalized graphene [41]. Such changes are consistent with the presence of residual sp^3 islands upon pressure release. DFT calculations on partially functionalized structures (Supplemental Information in Ref. [5]) predict stable structures upon pressure release, depending on the spatial distribution of the chemical groups, while other configurations lead to unstable structures. Therefore, for a random distribution of chemical groups upon phase transition, it is possible that only some regions will retain the sp^3 configuration upon pressure release. However, it is important to state that the possibility that the D and D′ bands are activated by other sources of structural defects cannot be ruled out.

To glean further insight into the experimental results, we carried out MD simulations to dynamically follow the restructuring process at a given temperature, and DFT calculations to study the stacking order of the rehybridized structure and the interplay between structural and electronic properties. Both theoretical schemes assume a starting model of AB-stacked five-layer graphene whose top surface is covered with either −OH or −H groups. These are assumed to originate from water molecules in reactions under high pressures at the surface of graphene [5] (see details in Section 4 in Supplementary Information), and play a fundamental role in both the rehybridization and stabilization processes [42]. For simplicity, we considered the ideal case of a complete coverage from sp^3 groups to capture the phenomenology. The sp^2 to sp^3 phase transition is possible even for incomplete functionalization due to a cooperative effect in which the formation of a single sp^3 site induces the sp^2 to sp^3 conversion in lines across the flake [5]. Such incomplete functionalization of the top layer could generate structures with coexisting sp^2-sp^3 regions, and this topic has been addressed in Ref. [5].

Fig. 3(a) presents the profiles of three snapshots with increasing pressure obtained from MD simulations, clearly showing the evolution of sp^3 bond formation. Under compression, the phase transition starts with the inter-layer bonding between the first two layers, giving rise to diamondene. For the formation of covalent bonds between diamondene and the graphene layer underneath to occur, the pressure needs to be further increased since the distance between the layers is too large to allow for the rehybridization. In this process, which we refer to as vertical propagation, the third graphene layer displaces horizontally resulting in a transformation from an ABA to an ABB three-layer stacking configuration (see details in Sec. 5 in Supplemental Information).

The physical picture here is that for covalent bonds to be formed between diamondene and the third graphene layer, the carbon atoms of the third layer need to be displaced by one base vector so that they will be aligned with the dangling bonds from the carbon atoms of the second layer. A similar mechanism has been proposed in Bakharev et al. [11], to explain why they obtained evidence of F-diamane formation upon fluorination of AB bilayer graphene and no evidence of its formation was obtained upon fluorination of trilayer ABA graphene.

Fig. 3(b and c) show the optimized geometries for two configurations with increasing applied force, obtained from DFT calculations. In agreement with the MD simulations, the diamondene structure is initially formed with the underlying three-layer graphene protecting the array of dangling bonds [Fig. 3(b)]. Next, by increasing the applied forces, the sp^2-sp^3 process propagates through the other layers, resulting in a completely rehybridized five-layer geometry characterized by an ABBBB stacking, as shown in Fig. 3(c). The BB part of the stacking corresponds to the crystal structure of hexagonal diamond. The band structure corresponding to the ABBBB stacking, shown in Fig. 3(d), preserves the main features of diamondene, which are the localized states at the dangling bonds leading to a pair of spin-polarized bands. This proposed phase transition mechanism also includes the possibility of functionalization on both top and bottom sides (see Section 6 in the Supplemental Information).

Although our models employ an uniaxial pressure scheme, justified by the huge difference between in-plane and out of plane compressibility in graphene systems [16], our results can be extended to the hydrostatic case. In fact, by anchoring a three-layer graphene on a graphane substrate and applying periodic boundary conditions in a calculation which includes a predefined hydrostatic pressure, we found the same phenomenology (see Section 5 in the Supplemental Information). However, since the diamondene lattice constant (2.54 Å) is larger than that of graphene (2.49 Å), there is a competition between the vertical and lateral forces: while the former tends to induce the rehybridization, the latter makes the process more difficult. As a result, the hydrostatic pressure tends to slightly increase the critical pressure required for the transition.

Due to the importance of kinetic aspects, our DFT calculations do not aim to find the lowest energy configuration. Rather, given the initial conditions (interaction between graphene and −OH groups), our conclusion is that, in fact, mixed stacking orders are highly likely. In a systematic investigation of this problem, Xie et al. [64] have ascribed this hexagonal diamond order to a facile initial nucleation mechanism, involving the existence of coherent sp^2–sp^3 interfaces. Still according to their results, cubic diamond growth should have a much slower kinetics and should be mixed with that of hexagonal diamond.

The theoretical models show that compressing 5-layer graphene in the presence of passivation groups such as −H or −OH, leads to a surface-to-bulk phase transition mechanism. An in-situ detection of C–H or C–OH bonds does not seem to be feasible given their low Raman and infrared scattering cross-sections, added to a strong IR absorption from water PTM and incompatibility of the DAC with techniques such as X-ray photoelectron spectroscopy. However, we obtained experimental indications of the occurrence of this surface-to-bulk phase transition that further corroborates with the role of water to drive the phase transition. For instance, the fact that the onset of the phase transition is very similar for bi-layer

graphene, five-layer graphene and thin graphite, indicates that the onset does not strongly depends on the number of layers, being consistent with a process that rather depends on the surface in contact with water, initiating with the rehybridization of the top layers.

The role of the stacking order of flakes in the vertical propagation is discussed in Section 7 of the Supplemental Information. The results from high-pressure Raman measurements on an unsupported graphene powder (randomly stacked flakes) and unsupported graphite flake (defined stacking), as well as from X-ray diffraction data on the graphene powder - all samples compressed in a water PTM - suggests that higher pressures are necessary for the vertical propagation to occur for randomly-stacked flakes. Furthermore, those experiments indicate that the asymmetrical G band broadening after phase transition observed for some samples, (for instance, notice the G band shape for five-layer graphene and graphite at 4.5 GPa in Fig. 2), could be explained by Raman signals coming from the top sp^2-sp^3 and bottom sp^2 regions during the vertical propagation of the sp^2 to sp^3 reconstruction (see Fig. S8 of the Supplemental Information). However, it is important to mention that different C–C stretching modes related to C–H and/or C–OH functionalization [62,63] could also contribute to G band shape asymmetry after the onset of phase transition.

We now present the evidence of transparency and hardness and discuss how some of the features observed in these measurements can be explained by our model. Fig. 4(a) shows optical images of the sample inside of the DAC at different pressures. Starting around 4 GPa, a series of color changes occur in the graphite flake. We note that possible causes of optical changes such as delamination of the SiO_2 layer, flow of the solid PTM, and proximity of the top anvil with the sample should change the optical contrast over the whole silicon disk. However, our observed optical changes are mostly localized on the flakes. In fact, the optical changes in graphite are precisely confined into the flake's boundaries. The main evidence that the optical changes are associated with structural changes in the flakes and not with other spurious effects is the fact that they are correlated with changes in Raman spectra, which we have already discarded to be caused by PTM/substrate interaction-related effects.

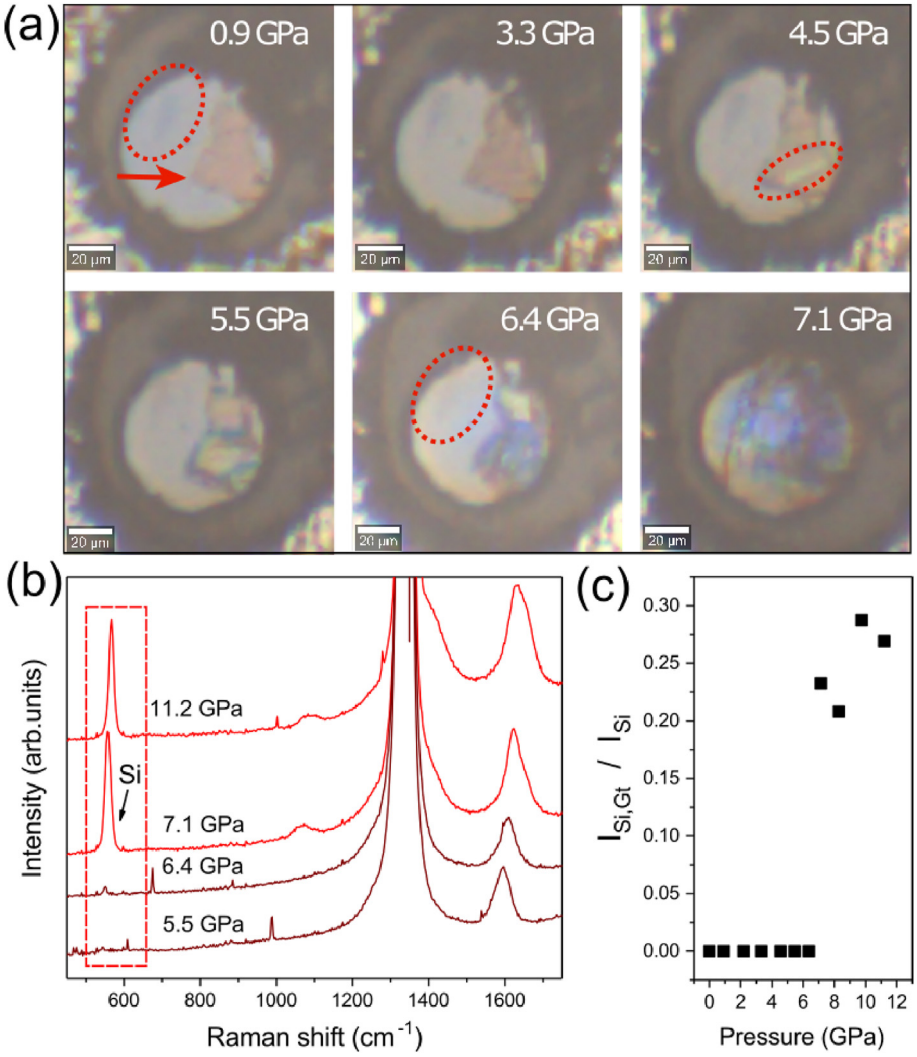

Fig. 4. Evidence of pressure-induced transparency. (a) Optical images of the 5-layer graphene sample and graphite inside of the DAC at different pressures. In the first panel (0.9 GPa), the five-layer graphene is highlighted by the dashed ellipse, and the graphite flake is indicated by the arrow. At 4.5 GPa, a color change occurs in the graphite flake, with the formation of a yellow strip. With increasing pressure to 5.5 GPa, the yellow region spreads over the graphite flake. At 6.4 GPa, the five-layer graphene flake turns transparent. The yellow color remains only at the top-half region of the graphite flake, and its bottom-half shows a color similar to the substrate - an indication of transparency. At 7.1 GPa, the color changing ends, and the flakes can no longer be seen. The subsequent color changes are likely related to fractures on the substrate, damaging the SiO_2 layer. (b) Raman spectra of graphite at different pressures. Notice that, from 7.1 GPa, the Raman peak from the silicon substrate appears at approximately 550 cm^{-1}. (c) Plot of the ratio between intensities of the silicon peak measured on graphite ($I_{Si,Gt}$) and on bare silicon substrate (I_{Si}). (A colour version of this figure can be viewed online.)

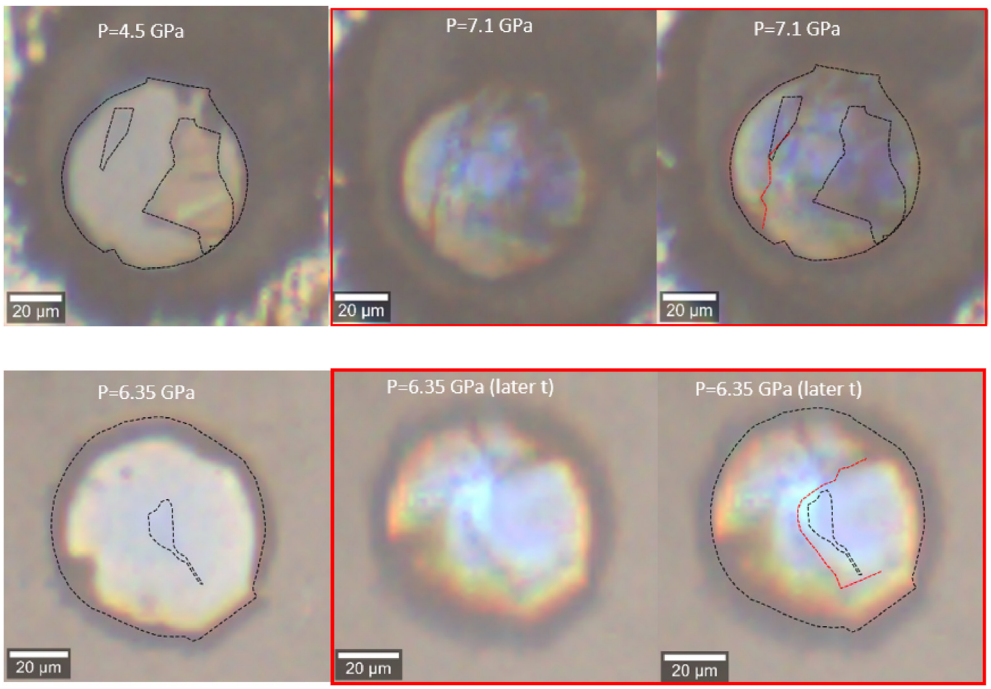

Fig. 5. Indications of the formation of a hard 2D phase from optical images. Optical images highlighting the flake contours by black dashed lines before (left) and after (right, inside red box) phase transition for five-layer (top row) and two-layer (bottom row) graphene. The silicon fractures are highlighted by the red-dashed lines in the panels at the right side. (A colour version of this figure can be viewed online.)

At 4.5 GPa, we have the formation of a yellow strip in graphite, which coincides with an abrupt broadening of G band followed by an increase in $d\omega_G/dP$ as well as an intensity suppression of 2D band above this pressure. Between 4 and 7 GPa we observed an increase in G bandwidth and subsequent increase in ω_G *vs P* slope for both five-layer graphene and graphite. In the same pressure range, the yellow region spreads over the graphite flake, then gradually turns to a color similar to the substrate - an indication of increasing transparency. The five-layer graphene and graphite flakes can no longer be seen at 6.4 GPa and 7.1 GPa, respectively. Also, after 7 GPa, we no longer observe drastic changes in the Raman spectra.

Thus, the optical changes shown in Fig. 4(a) are indications of transparency. The actual proof is provided by the Raman signal coming from the silicon substrate underneath the graphite flake after 7 GPa, as shown in Fig. 4(b). The fact that the Raman signal from silicon could be detected when we measured the graphite flake shows that incident laser field was able to reach the substrate throughout the flake, which became transparent due to structural changes (graphite is opaque to visible light). To further confirm and quantify this transparency event, Fig. 4(c) shows the plot of the ratio between the intensity of the Si Raman peak measured at the graphite flake, $I_{Si,Gt}$, and its intensity measured directly on the Si substrate, I_{Si}, as a function of pressure. As the graphic shows, the ratio becomes ≈ 0.25 for pressures above 7.1 GPa, indicating that the transparency is partial. However, care must be taken for not drawing further conclusions about the transparency of the new phase since optical absorption is wavelength dependent, and a quantitative connection of $I_{Si,Gt}/I_{Si}$ with the absolute value for the absorption at 532 nm is not straightforward. To the best of our knowledge, 7.1 GPa is the lowest pressure that transparency has been reported in room-temperature compressed graphite and, once again, we attribute it to the role of water in facilitating the phase-transition. For instance, such transparent phases have been reported at 18 GPa in graphite compressed in methanol/ethanol (4:1) [17] and potassium bromide [43] PTMs.

The optical changes observed in the graphite flake are in accordance with our surface-to-bulk phase transition model. The appearance of a yellow color over the graphite flake shown in Fig. 4(a) at $\approx$ 4 GPa would correspond to the phase transition of the top layers of graphite, since it would change the local optical contrast as the top layers become more transparent. This situation is illustrated in Fig. 3(a) (middle structure) and Fig. 3(b) for the rehybridization of the first two layers. As the pressure increases, according to our proposed mechanism, the vertical propagation evolves and the phase transition extends to deeper layers, as illustrated in Fig. 3(a) (bottom structure) and Fig. 3(c). This situation correlates with the observed change of color of the graphite flake upon pressure increase, which turns to a color similar to the substrate at 7 GPa.

From the optical images, we observed cracks on the substrate along directions defined by the edges of the five-layer (Fig. 5 top row) and bi-layer graphene samples (Fig. 5 bottom row). Notice that these cracks appear only at 6 GPa for bi-layer and at 7 GPa for five-layer, that is, after phase transition takes place. Such cracks were not observed for bare SiO_2/Si substrate compressed in the same pressure range (see Fig. S12 in the Supplemental Information). This suggests the formation of a hard 2D phase upon phase transition, capable of indenting and cleaving the substrate. In fact, in our surface-to-bulk phase transition model, the formation of a hard 2D phase compressing the graphene layers underneath provides a possible explanation for the increase in ω_G *vs P* observed for five-layer graphene and graphite after 4 GPa (see discussion in Sec. 9 in the Supplemental Information).

To confirm the formation of a hard phase upon compression, we compressed a new sample containing a four-layer graphene and a graphite flake on SiO_2/Si [Fig. 6(a)] in a DAC using water PTM, up to 8 GPa - pressure above the onset of phase transition according to our high-pressure Raman experiments. Fig. 6(b) shows the optical image of the recovered sample. Interestingly, the optical contrast of the four-layer graphene sample became much reduced, which could indicate that the sample detached from substrate upon

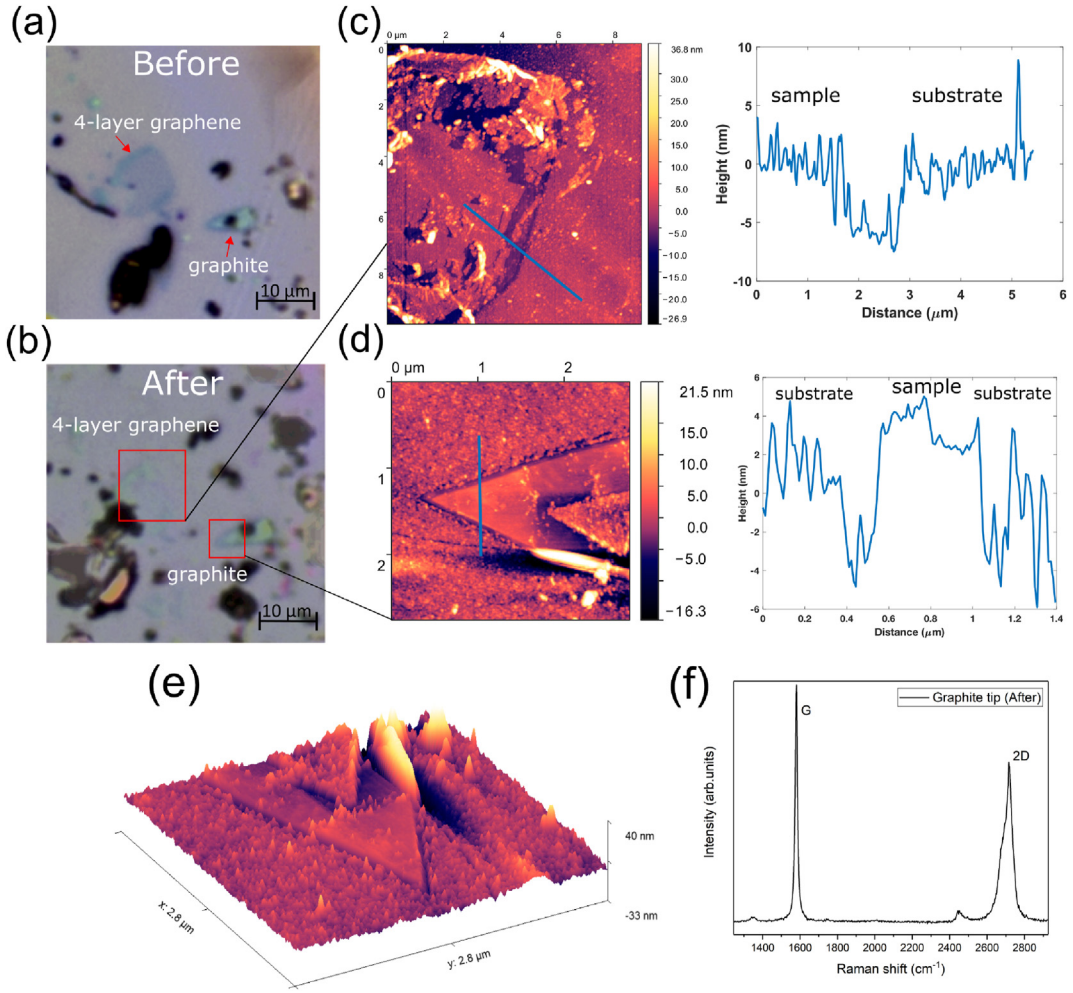

Fig. 6. Indentation marks on SiO_2 substrate from AFM topographic images. (a,b) Optical images with background correction of the graphite and four-layer graphene before (a) and after (b) compression up to 8 GPa. The flakes are identified by the red arrows in (a). The open squares in (b) indicate the regions where the AFM images were taken. (c,d) AFM topographic images of the four-layer graphene (c) and graphite (d) flakes after compression up to 8 GPa, showing deep grooves formed on the silicon oxide substrate along the edges of the flake. On the right side, the height profiles extracted along the blue lines in the images are shown. The height profiles show that the flakes are leveled with the substrate, indicating that they got sunk into the silicon dioxide layer. (e,f) 3D topographic AFM image from the tip of the graphite flake (e), and Raman spectra from same region (f), confirming the presence of many layers (more than 20). Therefore, one would expect the sample to be at least ~ 10 nm above substrate level, confirming that it penetrated the SiO_2 substrate. (A colour version of this figure can be viewed online.)

decompression. However, a Raman map of the region shows that the four-layer graphene samples remains there (Fig. S13 in the Supplemental Information). It is not clear the origin of this apparent increase in transparency for the four-layer graphene sample. It could be caused by irreversible changes in the sample or by damage of the SiO_2 substrate underneath the flake due to the indentation.

Atomic force microscopy (AFM) topographical images of the recovered sample containing the four-layer graphene and the graphite flake are exhibited in Fig. 6(c) and (d), respectively. The images show clear indentation marks on the SiO_2 substrate, as confirmed by the height profiles extracted from them (on the right). Notice that, from the AFM topographical profiles, the samples are leveled with the substrate, indicating that they got sunk into the silicon dioxide layer. This is evident from the AFM profile taken across the tip of graphite flake [Fig. 6(d) - right panel] and 3D topographic AFM image [Fig. 6(e)], showing that the sample is only ~ 3 nm above the substrate level. Raman spectra acquired at that same location [Fig. 6(f)], confirm the presence of many layers (more than 20), therefore we would expect the flake to be at least ~ 10 nm above the substrate level.

Given that hardness can be defined as a measure of the ability of a body to resist the penetration of another body, and given it is correlated with the nature of chemical bonding [44], it is quite surprising that the graphite sample penetrated the silicon dioxide upon compression, if one compares the weak van der Waals forces between the layers in graphite with the strong covalent bonds in SiO_2. The difference is clear if one compares the Vickers hardness (VHN) for graphite, 7–11 kgf/mm^2 [45], with VHN for amorphous SiO_2, 564.9 kgf/mm^2 [46]. In fact, nano-indentation experiments performed on graphene of different thicknesses on SiO_2, in an estimated local pressure range of 0–7 GPa, showed that graphene systems (1–3 layers and graphite) get deeper indentation marks if compared with SiO_2 [12] when subjected to the same tip-force, with deeper marks for thicker flakes. These nano-indentation experiments confirm that graphene systems are softer than SiO_2, when compressed under same conditions, therefore not being able to indent the silicon substrate as observed in our experiments.

Our results further confirm the occurrence of a phase transition with the formation of a pressure-induced phase with hardness superior to amorphous SiO_2, at least. Our previous analysis relies on the assumption that the rehybridization is accompanied by a

structural change which increases the material's hardness. Though expected due to the formation of a diamond-like structure, this hypothesis can be carefully checked by first principles calculations. For this purpose, we have carried out additional DFT calculations, and we found, indeed, interesting trends in the mechanical response of compressed few-layer graphene, which fully corroborate the presented reasoning. We focused on the OH-top-functionalized diamondene structure with the number of layers varying from 2 to 5. To quantify the discussion we determined, in each case, the bulk and Young moduli. It is important to point out that the bulk modulus directly correlates with Vickers hardness [47].

We found bulk moduli, calculated with the Birch-Murnaghan third-order equation of state [48], ranging from 444 (five-layer diamondene) to 466 GPa (bilayer diamondene), which are both slightly above the diamond's bulk modulus calculated with the same methodology (423 GPa, comparable to the experimental value of 443 GPa). Also, the Young moduli, calculated with strains applied along the zig-zag direction, are relatively high: we found 1.3 TPa in the five-layer case, and values close to 1.2 TPa in the other cases, with similar results for strains along the armchair direction. Finally, as a measure of hardness in the transverse direction, which is important to interpret indentation experiments, we determined the transverse Young modulus for each diamondene structure. We found a value as high as 1.1 TPa in the four-layer case, with similar results for the other thicknesses (0.93, 1.03 and 1.1 GPa for two, three- and five-layer diamondene, respectively). To compare with, Yang Gao et al. [7] found 0.99 TPa for a double-sided-H-functionalized bilayer diamond-like structure. Therefore, the DFT mechanical characterization suggests that the indentation features observed in the experiment may be ascribed to the formation of a 2D hard-phase diamond-like structure, for which the diamondene is a consistent representation.

5. Conclusion

Our combined experimental results indicate that compressing graphene systems in the presence of water leads to a structural phase transition to a phase containing sp^3 carbon at 6 GPa for bilayer graphene and between 4 and 7 GPa for five-layer graphene and graphite. The Raman evidence for bi-layer graphene comes from the simultaneous abrupt broadening and slight redshift of G band around 6 GPa, concomitant with drastic 2D band's redshift and intensity suppression. For five-layer graphene, the evidence comes from an abrupt broadening of G band around 4 GPa, followed by an increase in $d\omega_G/dP$ in the 4–7 GPa range, and eventual 2D band suppression at approx. 7 GPa. For graphite, the evidence comes from a G band broadening at 4 GPa and 2D band suppression above this pressure, as well as an increase in $d\omega_G/dP$ in the 4–7 GPa range. The new phase is transparent - as evidenced by changes in the optical contrast of the flakes, correlated with the observation of the Raman signal coming from the silicon substrate underneath the graphite flake - and hard - from indentation marks on the harder silicon oxide substrate. Those observations suggest the formation of a 2D diamond-like phase. Furthermore, theoretical models and experimental data indicate a surface-to-bulk phase transition, consistent with the formation of diamondene at the phase transition onset.

Further structural information is required to conclusively claim 2D diamond formation. The obtention of in-situ confirmation presents an enormous challenge in terms of low x-ray cross section, given the two-dimensional nature and low atomic number of the samples. Such a confirmation would require a stable material upon decompression, which could in principle be obtained by a complete functionalization of graphene's top surface, with one chemical group per graphene sublattice [5]. At room temperature, water is in the ice form above 1 GPa, and therefore this condition might not be met due to the low mobility of the water molecules. Thus, while a stable 2D diamond could be obtained through further tuning the synthesis parameters, e.g. by increasing temperature or improving sample-surface cleanness, to obtain diamondene is a matter of choice for the right substrate. Potential applications of diamondene are in 2D magnetism, gate-tunable spin-polarized currents, and spin-polarized photocurrents, with broad impact in both fundamental research and practical applications.

CRediT authorship contribution statement

Luiz G. Pimenta Martins: Conceptualization, Methodology, Validation, Formal analysis, Investigation, Data curation, Writing - original draft, Writing - review & editing, Visualization, Project administration. **Diego L. Silva:** Validation, Formal analysis, Investigation, Data curation, Visualization. **Jesse S. Smith:** Validation, Investigation, Resources. **Ang-Yu Lu:** Validation, Formal analysis, Investigation, Visualization. **Cong Su:** Investigation. **Marek Hempel:** Methodology, Investigation. **Connor Occhialini:** Formal analysis, Investigation. **Xiang Ji:** Investigation. **Ricardo Pablo:** Investigation. **Rafael S. Alencar:** Investigation. **Alan C.R. Souza:** Software, Validation, Formal analysis, Investigation. **Alysson A. Pinto:** Software, Validation, Formal analysis, Investigation. **Alan B. de Oliveira:** Methodology, Software, Validation, Formal analysis, Investigation, Resources, Data curation, Writing - original draft. **Ronaldo J.C. Batista:** Methodology, Software, Validation, Formal analysis, Investigation, Resources, Data curation. **Tomás Palacios:** Resources. **Mário S.C. Mazzoni:** Conceptualization, Methodology, Software, Validation, Formal analysis, Investigation, Resources, Data curation, Writing - original draft, Writing - review & editing. **Matheus J.S. Matos:** Methodology, Software, Validation, Formal analysis, Investigation, Resources, Data curation. **Riccardo Comin:** Resources, Validation, Supervision. **Jing Kong:** Conceptualization, Methodology, Validation, Resources, Writing - review & editing, Supervision, Funding acquisition. **Luiz G. Cançado:** Conceptualization, Validation, Investigation, Resources, Writing - original draft, Writing - review & editing, Supervision, Project administration, Funding acquisition.

Declaration of competing interest

The authors declare that they have no known competing financial interests or personal relationships that could have appeared to influence the work reported in this paper.

Acknowledgements

We are grateful to P. Jarillo-Herrero for granting lab access for sample fabrication, and J. Deng, L. Xie, A.P.M. Barboza, L. Dresselhaus-Copper and L. Ju for fruitful discussions. L.G.P.M. and J. K. acknowledge the support from National Science Foundation (NSF) under the EFRI2-DARE program (EFMA-1542863). L.G.P.M.,M.H., T.P. and J.K. acknowledge the support from AFOSR FATE MURI, grant no. FA9550-15-1-0514. L.G.P.M. and J.K. ackowledge the support from CNPQ under the program Ciência sem Fronteiras (206251/2014–9). R.C. acknowledges support from the Alfred P. SloanFoundation. L.G.C. acknowledges the support from CODEMGE. L.G.C., M.S.C.M., A.C.R.S.,M.J.S.M., A.B.O. and R.J.C.B. acknowledge the support from CNPq and FAPEMIG. A.B.O., A.C.R.S., L.G.C, M.J.S.M., M.S.C.M. and R.J.C.B. acknowledge the support from INCT-Nano-Carbono. M.J.S.M., A.B.O. and R.J.C.B. acknowledge the support from Universidade Federal de Ouro Preto (UFOP). M.S.C.M., M.J.S.M, A. C. R. S. and A. A. P. acknowledges financial support from

CAPES - Finance Code 001. We acknowledge computational support from LCC-CENAPAD-UFMG and CESUP-UFRGS. This work was performed in part at the Center for Nanoscale Systems (CNS), a member of the National Nanotechnology Coordinated Infrastructure Network (NNCI), which is supported by the National Science Foundation under NSF award no. 1541959. Synchrotron x-ray diffraction was performed at HPCAT (Sector 16), Advanced Photon Source (APS), Argonne National Laboratory. HPCAT operations are supported by DOE-NNSA's Office of Experimental Sciences. The Advanced Photon Source is a U.S. Department of Energy (DOE) Office of Science User Facility operated for the DOE Office of Science by Argonne National Laboratory under Contract No. DE-AC02-06CH11357. The high-pressure Raman measurements were performed at LCPNano – Laboratório de Caracterização e Processamento de Nanomateriais da UFMG. The authors acknowledge the MGgraphene Project for providing graphene powder samples and related AFM data.

Appendix A. Supplementary data

Supplementary data to this article can be found online at https://doi.org/10.1016/j.carbon.2020.11.038.

References

[1] Z. Zhao, B. Xu, Y. Tian, Recent advances in superhard materials, Annu. Rev. Mater. Res. 46 (2016) 383–406.
[2] A.A. Balandin, Thermal properties of graphene and nanostructured carbon materials, Nat. Mater. 10 (8) (2011) 569.
[3] L.A. Chernozatonskii, P.B. Sorokin, A.G. Kvashnin, D.G. Kvashnin, Diamond-like c 2 h nanolayer, diamane: simulation of the structure and properties, J. Exp. Theor. Phys. 90 (2) (2009) 134–138.
[4] L.A. Chernozatonskii, P.B. Sorokin, A.A. Kuzubov, B.P. Sorokin, A.G. Kvashnin, D.G. Kvashnin, P.V. Avramov, B.I. Yakobson, Influence of size effect on the electronic and elastic properties of diamond films with nanometer thickness, J. Phys. Chem. C 115 (1) (2010) 132–136.
[5] A.P. Barboza, M.H. Guimarães, D.V. Massote, L.C. Campos, N.M. Barbosa Neto, L.G. Cançado, R.G. Lacerda, H. Chacham, M.S. Mazzoni, B.R. Neves, Room-temperature compression-induced diamondization of few-layer graphene, Adv. Math. 23 (27) (2011) 3014–3017.
[6] L.Y. Antipina, P.B. Sorokin, Converting chemically functionalized few-layer graphene to diamond films: a computational study, J. Phys. Chem. C 119 (5) (2015) 2828–2836.
[7] Y. Gao, T. Cao, F. Cellini, C. Berger, W.A. De Heer, E. Tosatti, E. Riedo, A. Bongiorno, Ultrahard carbon film from epitaxial two-layer graphene, Nat. Nanotechnol. 13 (2) (2018) 133.
[8] F. Piazza, K. Gough, M. Monthioux, P. Puech, I. Gerber, R. Wiens, G. Paredes, C. Ozoria, Low temperature, pressureless sp2 to sp3 transformation of ultra-thin, crystalline carbon films, Carbon 145 (2019) 10–22.
[9] L.G.P. Martins, M.J. Matos, A.R. Paschoal, P.T. Freire, N.F. Andrade, A.L. Aguiar, J. Kong, B.R. Neves, A.B. de Oliveira, M.S. Mazzoni, et al., Raman evidence for pressure-induced formation of diamondene, Nat. Commun. 8 (1) (2017) 96.
[10] F. Piazza, M. Monthioux, P. Puech, I.C. Gerber, Towards a better understanding of the structure of diamanoïds and diamanoïd/graphene hybrids, Carbon 156 (2020) 234–241.
[11] P.V. Bakharev, M. Huang, M. Saxena, S.W. Lee, S.H. Joo, S.O. Park, J. Dong, D.C. Camacho-Mojica, S. Jin, Y. Kwon, et al., Chemically induced transformation of chemical vapour deposition grown bilayer graphene into fluorinated single-layer diamond, Nat. Nanotechnol. 15 (1) (2020) 59–66.
[12] F. Cellini, F. Lavini, C. Berger, W. de Heer, E. Riedo, Layer dependence of graphene-diamene phase transition in epitaxial and exfoliated few-layer graphene using machine learning, 2D Mater. 6 (3) (2019), 035043.
[13] F. Ke, Y. Chen, K. Yin, J. Yan, H. Zhang, Z. Liu, S.T. John, J. Wu, H.-k. Mao, B. Chen, Large bandgap of pressurized trilayer graphene, Proc. Natl. Acad. Sci. Unit. States Am. 116 (19) (2019) 9186–9190.
[14] F. Ke, L. Zhang, Y. Chen, K. Yin, C. Wang, Y.-K. Tzeng, Y. Lin, H. Dong, Z. Liu, J.S. Tse, et al., Synthesis of atomically thin hexagonal diamond with compression, Nano Lett. 20 (8) (2020) 5916–5921.
[15] T. Yagi, W. Utsumi, M.-a. Yamakata, T. Kikegawa, O. Shimomura, High-pressure in situ x-ray-diffraction study of the phase transformation from graphite to hexagonal diamond at room temperature, Phys. Rev. B 46 (10) (1992) 6031.
[16] M. Hanfland, H. Beister, K. Syassen, Graphite under pressure: equation of state and first-order Raman modes, Phys. Rev. B 39 (17) (1989) 12598.
[17] W. Utsumi, T. Yagi, Light-transparent phase formed by room-temperature compression of graphite, Science 252 (5012) (1991) 1542–1544.
[18] W.L. Mao, H.-k. Mao, P.J. Eng, T.P. Trainor, M. Newville, C.-c. Kao, D.L. Heinz, J. Shu, Y. Meng, R.J. Hemley, Bonding changes in compressed superhard graphite, Science 302 (5644) (2003) 425–427.
[19] M. Hanfland, K. Syassen, R. Sonnenschein, Optical reflectivity of graphite under pressure, Phys. Rev. B 40 (3) (1989) 1951.
[20] R. Aust, H. Drickamer, Carbon: a new crystalline phase, Science 140 (3568) (1963) 817–819.
[21] A. Ferrari, J. Robertson, Resonant Raman spectroscopy of disordered, amorphous, and diamondlike carbon, Phys. Rev. B 64 (7) (2001), 075414.
[22] A.P. Barboza, M.J. Matos, H. Chacham, R.J. Batista, A.B. de Oliveira, M.S. Mazzoni, B.R. Neves, Compression-induced modification of boron nitride layers: a conductive two-dimensional bn compound, ACS Nano 12 (6) (2018) 5866–5872.
[23] J.I.-J. Wang, Y. Yang, Y.-A. Chen, K. Watanabe, T. Taniguchi, H.O. Churchill, P. Jarillo-Herrero, Electronic transport of encapsulated graphene and wse2 devices fabricated by pick-up of prepatterned hbn, Nano Lett. 15 (3) (2015) 1898–1903.
[24] A. Jorio, M.S. Dresselhaus, R. Saito, G. Dresselhaus, Raman Spectroscopy in Graphene Related Systems, John Wiley & Sons, 2011.
[25] M. Huang, H. Yan, C. Chen, D. Song, T.F. Heinz, J. Hone, Phonon softening and crystallographic orientation of strained graphene studied by Raman spectroscopy, Proc. Natl. Acad. Sci. Unit. States Am. 106 (18) (2009) 7304–7308.
[26] J.E. Proctor, E. Gregoryanz, K.S. Novoselov, M. Lotya, J.N. Coleman, M.P. Halsall, High-pressure Raman spectroscopy of graphene, Phys. Rev. B 80 (7) (2009), 073408.
[27] K. Filintoglou, N. Papadopoulos, J. Arvanitidis, D. Christofilos, O. Frank, M. Kalbac, J. Parthenios, G. Kalosakas, C. Galiotis, K. Papagelis, Raman spectroscopy of graphene at high pressure: effects of the substrate and the pressure transmitting media, Phys. Rev. B 88 (4) (2013), 045418.
[28] B. Olinger, P.M. Halleck, Compression and bonding of ice vii and an empirical linear expression for the isothermal compression of solids, J. Chem. Phys. 62 (1) (1975) 94–99.
[29] G. Piermarini, S. Block, J. Barnett, Hydrostatic limits in liquids and solids to 100 kbar, J. Appl. Phys. 44 (12) (1973) 5377–5382.
[30] E. Wolanin, P. Pruzan, J. Chervin, B. Canny, M. Gauthier, D. Häusermann, M. Hanfland, Equation of state of ice vii up to 106 gpa, Phys. Rev. B 56 (10) (1997) 5781.
[31] D. Machon, C. Bousige, R. Alencar, A. Torres-Dias, F. Balima, J. Nicolle, G. de Sousa Pinheiro, A.G. Souza Filho, A. San-Miguel, Raman scattering studies of graphene under high pressure, J. Raman Spectrosc. 49 (1) (2018) 121–129.
[32] M. Amsler, J.A. Flores-Livas, L. Lehtovaara, F. Balima, S.A. Ghasemi, D. Machon, S. Pailhès, A. Willand, D. Caliste, S. Botti, et al., Crystal structure of cold compressed graphite, Phys. Rev. Lett. 108 (6) (2012), 065501.
[33] Y. Wang, J.E. Panzik, B. Kiefer, K.K. Lee, Crystal structure of graphite under room-temperature compression and decompression, Sci. Rep. 2 (2012) 520.
[34] E.M. Ferreira, M.V. Moutinho, F. Stavale, M. Lucchese, R.B. Capaz, C. Achete, A. Jorio, Evolution of the Raman spectra from single-, few-, and many-layer graphene with increasing disorder, Phys. Rev. B 82 (12) (2010), 125429.
[35] Q. Li, Y. Ma, A.R. Oganov, H. Wang, H. Wang, Y. Xu, T. Cui, H.-K. Mao, G. Zou, Superhard monoclinic polymorph of carbon, Phys. Rev. Lett. 102 (17) (2009) 175506.
[36] K. Umemoto, R.M. Wentzcovitch, S. Saito, T. Miyake, Body-centered tetragonal c4: a viable sp3carbon allotrope, Phys. Rev. Lett. 104 (12) (2010) 125504.
[37] J.-T. Wang, C. Chen, Y. Kawazoe, Low-temperature phase transformation from graphite to sp3orthorhombic carbon, Phys. Rev. Lett. 106 (7) (2011), 075501.
[38] F.J. Ribeiro, P. Tangney, S.G. Louie, M.L. Cohen, Structural and electronic properties of carbon in hybrid diamond-graphite structures, Phys. Rev. B 72 (21) (2005) 214109.
[39] D. Stojkovic, P. Zhang, P.E. Lammert, V.H. Crespi, Collective stabilization of hydrogen chemisorption on graphenic surfaces, Phys. Rev. B 68 (19) (2003) 195406.
[40] A.C. Ferrari, Raman spectroscopy of graphene and graphite: disorder, electron–phonon coupling, doping and nonadiabatic effects, Solid State Commun. 143 (1–2) (2007) 47–57.
[41] D.C. Elias, R.R. Nair, T. Mohiuddin, S. Morozov, P. Blake, M. Halsall, A.C. Ferrari, D. Boukhvalov, M. Katsnelson, A. Geim, et al., Control of graphene's properties by reversible hydrogenation: evidence for graphane, Science 323 (5914) (2009) 610–613.
[42] S. Paul, K. Momeni, Mechanochemistry of stable diamane and atomically thin diamond films synthesis from bi-and multilayer graphene: a computational study, J. Phys. Chem. C 123 (25) (2019) 15751–15760.
[43] E. Miller, D.C. Nesting, J.V. Badding, Quenchable transparent phase of carbon, Chem. Mater. 9 (1) (1997) 18–22.
[44] K. Herrmann, et al., Hardness Testing: Principles and Applications, ASM international, 2011.
[45] J.W. Anthony, Handbook of Mineralogy, vol. 4, Mineral Data Publishing, 1990.
[46] P. Shipway, I. Hutchings, The role of particle properties in the erosion of brittle materials, Wear 193 (1) (1996) 105–113.
[47] X.-Q. Chen, H. Niu, D. Li, Y. Li, Modeling hardness of polycrystalline materials and bulk metallic glasses, Intermetallics 19 (9) (2011) 1275–1281.
[48] F. Birch, Finite elastic strain of cubic crystals, Phys. Rev. 71 (11) (1947) 809, 1947.
[49] T.F. Fernandes, D.R. Miquita, E.M. Soares, A.P. Santos, L.G. Cançado, B.R. Neves, A semi-automated general statistical treatment of graphene systems, 2D Mater. 7 (2) (2020), 025045.
[50] H. Mao, J.-A. Xu, P. Bell, Calibration of the ruby pressure gauge to 800 kbar under quasi-hydrostatic conditions, J. Geophys. Res.: Sol. Earth 91 (B5) (1986)

4673–4676.
[51] D.L. Silva, J.L.E. Campos, T.F. Fernandes, J.N. Rocha, L.R. Machado, E.M. Soares, D.R. Miquita, H. Miranda, C. Rabelo, O.P.V. Neto, et al., Raman spectroscopy analysis of number of layers in mass-produced graphene flakes, Carbon 161 (2020) 181–189.
[52] S. Plimpton, Fast parallel algorithms for short-range molecular dynamics, J. Comput. Phys. 117 (1) (1995) 1–19, 1995.
[53] S.J. Stuart, A.B. Tutein, J.A. Harrison, A reactive potential for hydrocarbons with intermolecular interactions, J. Chem. Phys. 112 (14) (2000) 6472–6486.
[54] S. Nosé, A unified formulation of the constant temperature molecular dynamics methods, J. Chem. Phys. 81 (1) (1984) 511–519.
[55] P. Hohenberg, W. Kohn, Inhomogeneous electron gas, Phys. Rev. 136 (3B) (1964) B864.
[56] W. Kohn, L.J. Sham, Self-consistent equations including exchange and correlation effects, Phys. Rev. 140 (4A) (1965) A1133.
[57] J.M. Soler, E. Artacho, J.D. Gale, A. García, J. Junquera, P. Ordejón, D. Sánchez-Portal, The siesta method for ab initio order-n materials simulation, J. Phys. Condens. Matter 14 (11) (2002) 2745.
[58] N. Troullier, J.L. Martins, Efficient pseudopotentials for plane-wave calculations, Phys. Rev. B 43 (3) (1991) 1993.
[59] L. Kleinman, D. Bylander, Efficacious form for model pseudopotentials, Phys. Rev. Lett. 48 (20) (1982) 1425.
[60] J.P. Perdew, K. Burke, M. Ernzerhof, Generalized gradient approximation made simple, Phys. Rev. Lett. 77 (18) (1996) 3865.
[61] A. Kokalj, Computer graphics and graphical user interfaces as tools in simulations of matter at the atomic scale, Comput. Mater. Sci. 28 (2) (2003) 155–168.
[62] P. Vecera, J.C. Chacón-Torres, T. Pichler, S. Reich, H.R. Soni, A. Görling, K. Edelthalhammer, H. Peterlik, F. Hauke, A. Hirsch, Precise determination of graphene functionalization by in situ Raman spectroscopy, Nat. Commun. 8 (1) (2017) 1–9.
[63] B. Ma, R. Rodriguez, D. Raul, A. Ruban, S. Pavlov, E. Sheremet, The correlation between electrical conductivity and second-order Raman modes of laser-reduced graphene oxide, Phys. Chem. Chem. Phys. 21 (19) (2019) 10125–10134.
[64] Y.-P. Xie, X.-J. Zhang, Z.-P. Liu, Graphite to diamond: origin for kinetics selectivity, J. Am. Chem. Soc. 139 (7) (2017) 2545–2548.